Soft Matter

ROYAL SOCIETY OF CHEMISTRY

PAPER

View Article Online
View Journal | View Issue

Cite this: *Soft Matter*, 2025, **21**, 8704

Toughening 3D printed elastomers using mechanophore crosslinkers

Ana Paula Kitos Vasconcelos,[a] Nicholas J. Van Zee,[b] Allison Rattay,[a] Aileen Y. Sun,[c] Yunxin Yao,[b] S. Cem Millik,[a] Claire J. Ogilvie,[b] Ayokunle Olanrewaju,[c] Stephen L. Craig *[b] and Alshakim Nelson *[a]

Received 5th September 2025,
Accepted 25th October 2025

DOI: 10.1039/d5sm00904a

rsc.li/soft-matter-journal

Elastomeric materials are widely used in industrial application sectors including construction, automotives, soft robotics, and biomedicine. Light-based three-dimensional (3D) printing enables the manufacturing of elastomeric polymer networks with geometric and functional customizability beyond the capabilities of traditional manufacturing methods. These 3D printed polymer networks often suffer from premature mechanical failure of the material that limits their viability in load-bearing applications. One approach to toughen elastomers is to employ non-covalent additives as sacrificial bonds in the polymer network; however, this toughness enhancement comes with a trade-off in the stiffness of the resultant object. Herein, we use a 1 : 1 substitution of cyclobutane-based mechanophores as scissile covalent crosslinks in 3D printed poly(methoxyethylacrylate) networks to enhance the material toughness without compromising stiffness. These crosslinkers increased the material's toughness in tensile and tearing tests without altering its stiffness or appearance. The enhanced toughness and tear resistance of these elastomers enabled bonding operations such as stitching and suturing. The results suggest that mechanophores offer a promising route to toughen 3D printed elastomers.

Introduction

Three-dimensional (3D) printing has emerged as a powerful manufacturing technique for creating polymeric objects on-demand from digital design models. Among the various 3D printing methods, vat photopolymerization has garnered significant attention due to its high resolution, fast printing speed, and geometric versatility.[1] Vat photopolymerization uses a photopolymerizable liquid resin precursor, and a light source is used to selectively cure the resin layer-by-layer in pre-programmed locations to yield a three-dimensional polymer network-based object.[2,3] Digital light processing (DLP), a subtype of vat photopolymerization, utilizes a selectively projected light source to cure an entire resin layer simultaneously, making it one of the most time-efficient and widely adopted 3D printing techniques.[4] DLP's customizability as well as high resolution and fast rates of printing have increased its popularity as a printing method, where it has established a strong presence in the medical and manufacturing fields to fabricate dental molds and medical devices, as well as parts for on-demand production and prototyping.[5,6]

Acrylate-based thermosetting resins are ubiquitous in the vat photopolymerization 3D printing field due to their availability, low viscosity, mechanical and functional versatility, and rapid polymerization rates.[7] Acrylate resins undergo rapid radical polymerization to form a crosslinked polymer network that can be brittle in nature.[8] Network brittleness can be caused by network heterogeneity[9] (*i.e.*, differing polymer strand lengths between crosslinks) where stress concentrates on a small fraction of short chains leading to fracture.[10] These defects are further exacerbated by the layer-by-layer fabrication inherent in 3D printing, due to reduced interlayer adhesion.[11] Toughening acrylate-based materials is of interest to resist premature breakage, reduce waste by affording longer object lifespan, and imparting more functional versatility in printed elastomers.

To overcome the mechanical limitations, previous approaches have aimed to enhance polymer network toughness by increasing network homogeneity, altering crosslinking density, or incorporating energy dissipative groups.[12,13] These strategies, however, often sacrifice material stiffness due to the inversely correlated relationship between Young's Modulus and extensibility.[14] This inherent challenge makes it difficult to toughen a material without sacrificing stiffness and mechanical strength, complicating the ultimate application of a

[a] *Department of Chemistry and Molecular Engineering & Science Institute, University of Washington, Seattle, WA 98195, USA. E-mail: alshakim@uw.edu*
[b] *Department of Chemistry, Duke University, Durham, NC, 27708, USA. E-mail: stephen.craig@duke.edu*
[c] *Department of Bioengineering, University of Washington, Seattle, WA 98195, USA*

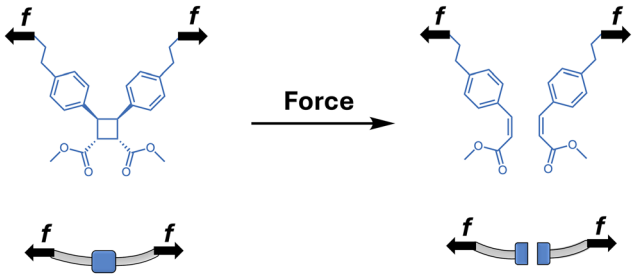

Fig. 1 Bond breaking mechanism of *cis*-diaryl substituted cyclobutane based mechanophore, *via* a force-coupled [2+2] cycloreversion to yield the corresponding cinnamates.

material that requires specifically defined strength and stiffness. Energy dissipating networks based on dynamic covalent bonds,[15] non-covalent bonds,[16,17] metal–ligand coordination,[18] hydrogen bonding,[19] and ionic bonding[20] can enhance toughness but usually reduce stiffness due to the weak nature of these bonding interactions.[21]

An alternative strategy is to use sacrificial covalent bonds, *i.e.* mechanophores, as both crosslinkers and toughening agents, which obviates the commonly encountered trade-off between stiffness and toughness. Wang *et al.* demonstrated that using force-responsive scissile mechanophores as crosslinkers in elastomers can significantly increase tear resistance without compromising material stiffness.[21] At the molecular level, the mechanophore crosslinker based on *cis*-diaryl substituted cyclobutane (Fig. 1) undergoes a force-coupled [2+2] cycloreversion that occurs when sufficient tension is generated in the crosslinking junctions. The scission of the mechanophore increases the distance between crosslinkers in the strands of highest tension within the network (*i.e.*, the strands that are at risk of breaking) and allows more energy to be stored in those strands before scission occurs. In other words, the mechanophores act as conventional crosslinkers in the bulk of the material, but in the small at-risk volumes of the network they act as sacrificial bonds that delay crack propagation. The force required to break the relatively weak diarylcyclobutane ring in the mechanophore crosslinker, determined by single molecule force spectroscopy,[22,23] is roughly five times lower than that of carbon–carbon single bonds in the network strands or in conventional, mechanically strong crosslinkers. Exactly how much force is required on average for dissociation depends on the substituents on the cyclobutane, the alignment of the reaction coordinate with the pulling axis, and the timescale at which dissociation occurs.[23] For lifetimes of 10^{-4} s, Wang *et al.* estimated the dissociation forces to be about 1 nN and 4.7 nN for the mechanophore employed here and conventional carbon–carbon bond, respectively. At lifetimes of 1 s, the relevant dissociation forces are approximately 0.7 and 4 nN.[21]

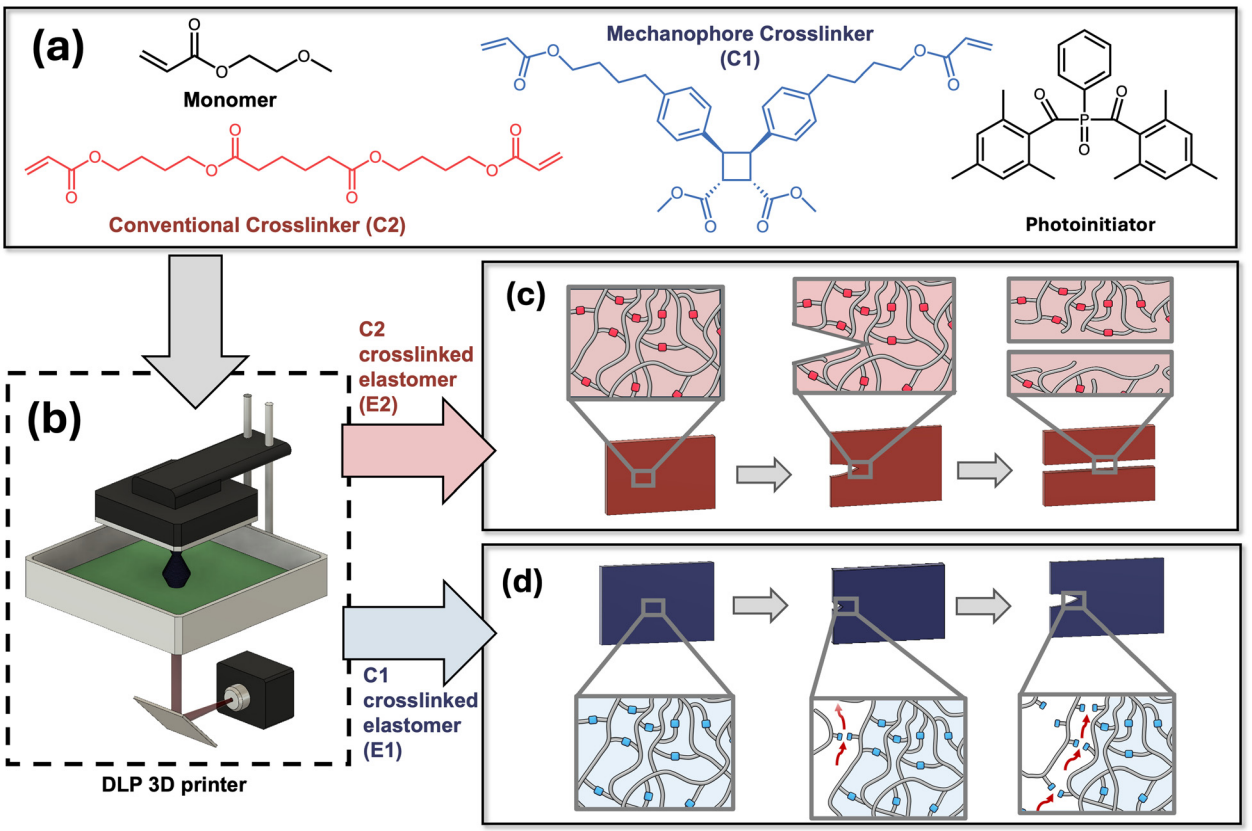

Fig. 2 (a) The components of the resin were 3D printed using a (b) DLP printer to form the elastomeric networks E1 and E2. (c) Network scission mechanism for E2 elastomer where crack propagates along crack plane. (d) Network scission mechanism for E1 elastomer where crack selectively breaks weak mechanophore crosslinker before primary chain.

The mechanical lability of the diarylcyclobutane drives its function as a sacrificial bond, and its incorporation in poly(methoxyethyl acrylate) networks increases the tear resistance up to nine-fold compared to the control elastomers that are crosslinked with a non-mechanophore strong crosslinker analogue. This molecular design strategy enables the enhancement of toughness, while maintaining modulus, swelling, and thermal behavior, which are indistinguishable from those of the control elastomers crosslinked with a non-mechanophore analogue.

We hypothesized that the substitution of conventional crosslinkers for their mechanophore-based analogues in photopolymer resins could toughen elastomers fabricated through light-based 3D printing *via* free radical polymerization while maintaining material stiffness. The work demonstrated by Wang *et al.* used cast samples synthesized *via* RAFT polymerization in an inert atmosphere, leading to greater control over the primary chain length and network topology. The toughening effect of the mechanophore crosslinker on the bulk material was highly primary chain length dependent—as the primary chains lengthen, the resultant tearing energies increased due to the elongation of the molecular path of the propagating cracks. Free radical polymerization is ubiquitous among light-based 3D printing resins, whereas controlled radical polymerization is rarely utilized beyond laboratory environments.[24,25] Therefore, this work seeks to expand the application space of mechanophore-based crosslinkers as a toughening strategy by demonstrating its utility in 3D printing *via* free radical polymerization.

Herein, we demonstrate that the stoichiometric substitution of conventional crosslinker C2 for mechanophore-containing crosslinker C1 increases the tensile toughness, compressive strength, and tear resistance of DLP 3D printed elastomers. These property enhancements were manifested without altering the stiffness of the material, avoiding the stiffness-toughness trade-off associated with other toughening strategies that incorporate sacrificial bonds. We showcase the enhanced toughness of the C1 elastomer by demonstrating that these materials – unlike the materials printed with the control C2 – can be bonded by stitching, which could be employed in applications such as medical training devices, soft robotics, and textiles.

Results and discussion

Formulation of resins

The liquid photopolymer resins were formulated with methoxyethyl acrylate (MEA) monomer with bisacyl phosphine oxide (BAPO) photoinitiator and either mechanophore crosslinker C1, or control crosslinker C2 (Fig. 2a). Details for crosslinker synthesis can be found in in the SI (Scheme S1 and Scheme S2). DLP 3D printing of the resins (Fig. 2b) produced elastomeric networks E2 (the C2-containing network) (Fig. 2c) and E1 (the C1-containing network) (Fig. 2d). BAPO was selected for its high absorbance at 405 nm, the printer wavelength, as well as its good solubility in the MEA monomer, enabling effective curing with visible light.[26] The resin containing C2 was used to verify

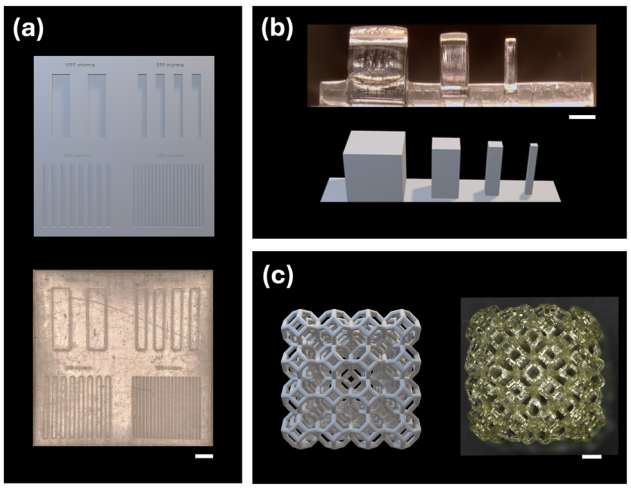

Fig. 3 (a) Computer-aided design (CAD) image of optimization model with 1 : 1 line-space arrays (left to right starting at top left) with void features that were 1000, 500, 250, 100 μm in width and 200 μm in depth and corresponding optical image of the printed structure. (b) CAD image of pillar array test structure (lower) and corresponding optical image (upper) of square pillars with widths of 1000, 500, 250 and 100 μm. The smallest pillar is missing on the far right in the optical image because the feature was too small to be printable. (c) CAD image and corresponding optical image of a Kelvin cell lattice. Scale bars are 1000 μm.

gelation and determine photo-parameters of the resin. Ultraviolet visible spectrophotometry (UV-vis) of C1 and C2-containing resins showed identical UV-vis profiles (Fig. S1). Photocuring experiments were performed on a rheometer equipped with a 405 nm light of an intensity of 20 mW cm^{-2} and the curing kinetics and gelation behavior were probed by monitoring the increase in storage modulus (G') upon irradiation. The resin was determined to be fully cured once G' reached a plateau, indicating the rapid formation of a fully cured elastic network at the printer wavelength and intensity (Fig. S2a).

The resin's curing depth and energy dose relationship were determined using a Jacobs working curve (eqn (1) and Fig. S2b). The working curve establishes the relationship between the intrinsic properties of the resin: the depth of penetration (D_p) and critical exposure energy (E_c), with surface exposure energy (E_0), the product of irradiation intensity and exposure time, and the ultimate curing depth (C_d) of the resin. Establishing the working curve allows for the determination of optimal exposure for a specific layer height and UV irradiance, which enables printing of this resin on a variety of 3D printers with tunable settings.

$$C_d = D_p \ln \frac{E_0}{E_c} \quad (1)$$

The working curve was determined using a protocol by Rau *et al.*,[27] where photorheology was used to determine the time for a 50 μm layer of resin to reach gel point when irradiated by 365 nm light. While the Asiga 3D printers in these experiments use 405 nm light for pattern wise exposure, the working curves that were determined using 365 nm light provides an estimate of the irradiation dose required. Thus, we started with 20 mW cm^{-2}

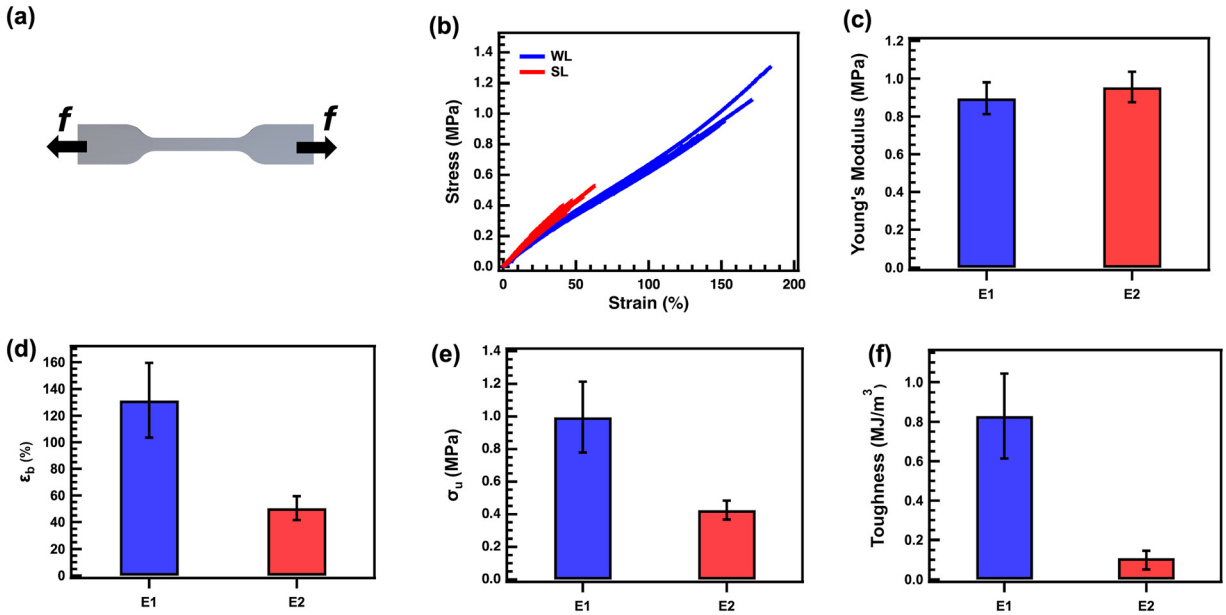

Fig. 4 The tensile properties were measured for E1 and E2 (a) dogbone specimens to yield their (b) characteristic stress–strain curves, which was used to determine the (c) Young's Modulus, (d) strain at break (ε_b), (e) ultimate tensile strength (σ_u), and (f) tensile toughness.

as the irradiation dose and further optimized prints using geometry optimization models and quantifying feature resolution.

DLP printing of elastomers

Printing was carried out using an AsigaMax DLP printer to synthesize networks E1 and E2. Using estimates from the Jacobs working curve, the resin formulation containing 2 mol% crosslinker and 0.3 mol% BAPO were printed with curing rates of 2 s per 50 μm layer. Detailed printing parameters can be found in Table S1. A test structure with an array of lines ranging from 100–1000 μm was printed (Fig. 3a). This test structure was used to optimize the exposure times as well as evaluate the resolution limit of the formulation. Printed structures demonstrated highly resolved channel features down to 100 μm in width without overcuring. Printed parts were inspected and imaged using optical profilometry with a Keyence VHX-970 digital microscope to analyze dimensional accuracy of the microfeatures (Fig. S3 and Table S2). An optimization model with varying pillar widths was printed to demonstrate the ability to print free-standing geometries as well as assess the resolution of these features (Fig. 3b). Pillars of 2000, 1000, and 500 μm were resolved but 250 μm pillars did not print successfully, indicating that the resin can be used to print highly resolved, free-standing features as low as 500 μm. Taking advantage of the geometric design freedom offered by DLP 3D printing, a Kelvin cell lattice structure was successfully printed (Fig. 3c), which demonstrates the ability to use this resin to produce architectures that are difficult to achieve through traditional, non-additive manufacturing methods.

Mechanical testing

Printed samples of E1 and E2 have near identical Young's moduli despite the different chemical composition of the crosslinkers. Resins containing either C1 or C2 were used to print specimens E1 and E2, respectively, for mechanical testing. Tensile dogbone specimens (ISO 37 Type 4[28]) (Fig. 4a) were printed, post-processed and tested under uniaxial tension on an Instron Load Frame to yield a characteristic stress–strain curve (Fig. 4b). E1 and E2 have indistinguishable Young's moduli of 0.9 ± 0.1 MPa and 0.90 ± 0.08 MPa (Fig. 4c), respectively, which demonstrates that the identity of the crosslinker does not influence the network topology (P = 34, Welch's t test). This conclusion is further supported by indistinguishable swelling behavior (Table S3). Rheometry revealed similar storage (G') and loss (G'') moduli over the angular frequency range of 0.1–100 rad s^{-1} (Fig. S4). Thus, the network connectivity of E1 and E2 is nearly identical despite the different cross-linkers used.

Whereas the low-strain properties of the printed specimens are indistinguishable, the high-strain properties are significantly different. E1 can be stretched further before breaking, displaying an elongation at break of 131.4% ± 28.0% compared to 50.0% ± 9.0% for E2 (Fig. 4d). The increased elongation at break in mechanophore-containing E1 corresponds to a greater ultimate tensile strength; 1.0 ± 0.2 MPa for E1 *vs.* 0.4 ± 0.1 MPa for E2 (Fig. 4e). The overall resistance to breaking can be quantified in terms of the greater tensile toughness of E1 relative to E2 (0.8 ± 0.2 MJ m^{-3} to 0.11 ± 0.04 MJ m^{-3}, respectively) (Fig. 4f). The enhanced properties observed in printed E1 were qualitatively consistent with the previous reports of similar mechanophore-crosslinked poly(methoxyethyl acrylate) materials formed by bulk fabrication. Under tension, the presence of the mechanophore crosslinker increased the ultimate tensile strength, elongation and toughness of E1 while maintaining the same Young's Modulus as E2 (Fig. S5 and Table S4).

The mechanical toughening from the mechanophore crosslinker was even more pronounced under uniaxial compressive

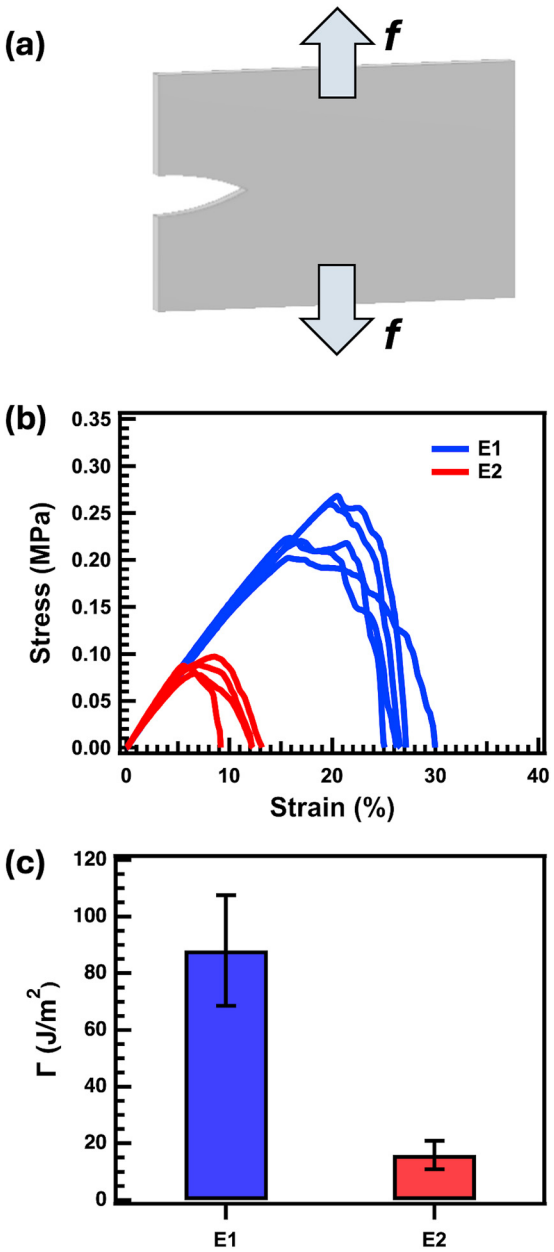

Fig. 5 The tear test according to the Rivalan-Thomas method on (a) notched elastomer samples in pure shear geometry, yielding (b) uniaxial extension stress–strain curves which was used to calculate (c) tearing energies for E1 and E2.

testing (Fig. S6 and Table S5). Compression of printed cylinders (2.5 mm diameter × 5 mm height) showed a similar trend to what was observed in tension. The printed E1 cylinders remained intact when compressed to a strain of 90%, whereas E2 cylinders of the same dimensions failed at 62.0% ± 4.9% strain. The ultimate compressive strength was about 65-fold higher for E1 than E2 (431.4 ± 2.8 MPa *vs.* 6.65 ± 0.01 MPa for E1 and E2, respectively). Significant mechanical enhancements were realized in E1 under compression, while still maintaining the same compressive modulus as E2 ($P = 0.32$, Welch's t-test). These results indicate that when a conventional covalent crosslinker C2 is substituted by the mechanically labile crosslinker C1, the high strain compressive properties are enhanced in 3D printed material specimens. The force-coupled crosslinker dissociation operates as a means of energy dissipation under both tensile and compressive forces without altering the moduli or topology of the network.

We performed tear testing experiments to investigate the response of these networks to macroscopic defects. Using the Rivlin-Thomas method,[29] we tested 3D printed and notched films using pure shear geometry (Fig. 5a) to determine tearing energy (Fig. S7). Failure of the material occurs *via* the propagation of pre-existing defects when the energy release rate at the crack tip exceeds the material's fracture energy, Γ (Fig. 5b).[30] The stress–strain curves show that the two elastomers have different critical strains for crack propagation and Γ of the mechanophore-containing E1 was 88.0 ± 19.5 J m^{-2}, with a mean value approximately 5.5 times higher than that of E2 15.9 ± 5.0 J m^{-2} (Fig. 5c). This improvement in toughness and tear resistance while maintaining moduli results from the force-induced cycloreversion of C1, which prolongs the path length of the propagating crack by preferential scission of the weak cyclobutane ring in the crosslinker over the network backbone, therefore increasing the primary chain length. The enhanced tearing energy observed in printed E1 compared to E2 are qualitatively consistent with that of the previously reported bulk fabricated materials that used controlled polymerization. The total magnitude of toughening is slightly lower for the 3D printed elastomers (~5.5 times higher tearing energy for printed E1 *vs.* E2) compared to the maximum effect reported in the literature for bulk networks fabricated using RAFT at the largest primary chain length examined (~9 times higher tearing energy for bulk fabricated E1 *vs.* E2 for primary chain lengths of 2000 repeats). The diminished magnitude of the toughening effect in the 3D printed specimens can be attributed to shorter or broader distribution of primary chain lengths associated with the free-radical polymerization process compared to the controlled RAFT process.[31] In the formulations employed here, the theoretical degree of polymerization along the primary network chains (assuming quantitative activation of the BAPO initiator) is 333, whereas the nine-fold toughening effect observed in the RAFT networks was obtained for average degree of polymerization of 2000. The primary chain lengths are not directly characterized in this work, and a full analysis is complicated by the fact that: (a) lower BAPO initiation would lead to higher average chain length, and (b) the fast rate of polymerization relative to initiation will lead to greater dispersity, with shorter chains contributing to lower toughness. Nonetheless, the controlled polymerization conditions of RAFT are impractical for most 3D printing applications, and the work reported here validates that common 3D printing conditions give network topologies that allow for significant mechanophore crosslinking effects to be realized.

Functional application of crosslinker substitution

We posited that the enhanced tear resistance of printed E1 specimens would transform the network into a suturable

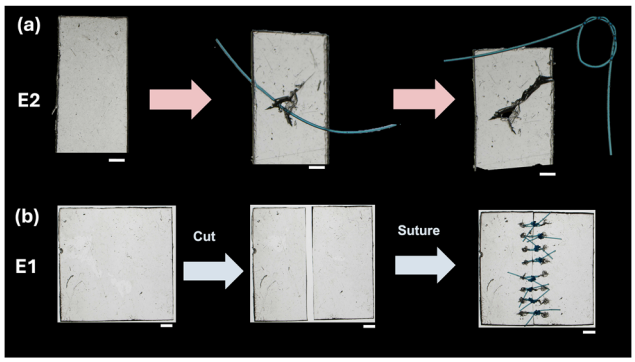

Fig. 6 Stitching of (a) E2 and (b) cutting and subsequent suturing of E1; scale bars are 1000 μm.

material. Suturable elastomers are of particular interest for the medical training field for medical practitioners and surgeons to learn proper suturing techniques.[32] Thus, 3D printed models that are suturable could be useful for this field. However, suturing printed elastomers can be challenging because the high concentration of stress during stitching can cause fracture propagation and material failure. The initial puncture creates a damage zone, and stress concentrates at the thread-material interface, often causing crack nucleation either from initial puncture, or from the tension applied to secure the suture.[33] This form of failure is observed, for example, when E2 is stitched with nylon suture thread (Fig. 6a). An overhand knot was tied with the suture thread and tightened to apply tension to the elastomer. For E2, puncturing of the material with the suture needle began to induce crack propagation, and the material failed during knot tightening due to crack initiation and propagation. In contrast, E1 withstood puncture and knotting without propagating cracks from the damage zone. This stitch retention is attributed to the increased resistance to failure imparted by the mechanophore crosslinker. Fig. 6b shows the successful cutting and stitching of E1. This functionality suggests that E1 could be used in multi-material systems for suturable medical training devices,[34,35] soft robotics,[36] as well as textile integrated materials.[37]

Conclusions

This work demonstrates the successful translation of mechanophore-based toughening strategies to 3D printing, which helps address some of the mechanical challenges that are inherent to additive manufacturing. In 3D printing, parts are often fabricated with fine structural features and small cross-sectional dimensions that are more susceptible to mechanical failure. Compared to non-additive manufacturing methods, the 3D printing process has a higher probability of creating small defects that can compromise the mechanical integrity of the printed components. A 1 : 1 substitution of a conventional crosslinker (C2) with a cyclobutane-based mechanophore crosslinker (C1) enhances the tensile toughness, compressive strength, and tear resistance without compromising stiffness, swelling or printability, overcoming the common trade-off between stiffness and toughness. The acrylate chemistry enables a ''drop-in'' replacement of the crosslinker with no change in the modulus, preserving properties that are often carefully optimized for performance while allowing higher elongation and load before failure. This results in a mechanically robust, damage resistant, and suturable material suited for applications where localized stresses along cracks or deformation zones are common, including medical models, soft robotics, textile-integrated systems and automotive or aerospace components. While the potential cost of cinnamate dimers employed in this work might limit their use in certain applications, recent advances in mechanophore design and discovery suggest that commercial advances might be realized by balancing cost and performance needs. The observation that even single-atom substitutions within crosslinkers are capable of meaningful changes in toughness provides additional reason for optimism.[38] Molecular-level enhancement of toughness *via* mechanophore crosslinking provides a promising route toward next-generation 3D printed elastomers that retain fidelity under mechanically demanding conditions.

Author contributions

A. P. K. V., N. J. V. Z., A. R., S. L. C. and A. N conceived the project and designed the experiments. A. N. and S. L. C. oversaw the project. N. J. V. Z. and C. J. O synthesized the crosslinkers. A. P. K. V. and A. R. performed 3D printing, rheology, tensile and compression experiments. Y. Y. performed tear testing and aided in data analysis. A. Y. S. collected Keyence Microscope images. S. C. M. aided in suturing. A. P. K. V. and A. N. wrote the manuscript with contributions from all authors.

Conflicts of interest

There are no conflicts to declare.

Data availability

The experimental procedures and characterization data supporting this article have been included as part of the supplementary information (SI). See DOI: **https://doi.org/10.1039/d5sm00904a**.

Acknowledgements

S. L. C. and A. N. were supported by the NSF Center for the Chemistry of Molecularly Optimized Networks (MONET; Award CHE-2116298). A. O. thanks the NSF Emerging Frontiers in Research and Innovation award 2223537, for support on this project. C. O. acknowledges support from the NIH through a training grant T32GM144291.

References

1 M. Layani, X. Wang and S. Magdassi, *Adv. Mater.*, 2018, **30**, 1706344.
2 A. Bagheri and J. Jin, *ACS Appl. Polym. Mater.*, 2019, **1**, 593–611.
3 Y. Gu, J. Zhao and J. A. Johnson, *Angew. Chem., Int. Ed.*, 2020, **59**, 5022–5049.
4 D. Chekkaramkodi, L. Jacob, R. Umer and H. Butt, *Addit. Manuf.*, 2024, **86**, 104189.
5 A. P. K. Vasconcelos, S. C. Millik, A. Vazquez, N. Sadaba, S. Sateesh, S. Daily, S. Yu, M. Zhang, N. Manitsirisuk and A. Nelson, *Annu. Rev. Mater. Res.*, 2025, **55**, 491–521.
6 M. A. Ghanem, A. Basu, R. Behrou, N. Boechler, A. J. Boydston, S. L. Craig, Y. Lin, B. E. Lynde, A. Nelson, H. Shen and D. W. Storti, *Nat. Rev. Mater.*, 2021, **6**, 84–98.
7 A. Bagheri and J. Jin, *ACS Appl. Polym. Mater.*, 2019, **1**, 593–611.
8 J. Steindl, T. Koch, N. Moszner and C. Gorsche, *Macromolecules*, 2017, **50**, 7448–7457.
9 S. P. O. Danielsen, H. K. Beech, S. Wang, B. M. El-Zaatari, X. Wang, L. Sapir, T. Ouchi, Z. Wang, P. N. Johnson, Y. Hu, D. J. Lundberg, G. Stoychev, S. L. Craig, J. A. Johnson, J. A. Kalow, B. D. Olsen and M. Rubinstein, *Chem. Rev.*, 2021, **121**, 5042–5092.
10 A. Arora, *Macromolecules*, 2025, **58**, 1143–1155.
11 K. P. Qin, A. Herzog-Arbeitman, W. Zou, S. Chakraborty, S. L. Kristufek, K. E. L. Husted, G. D. Joly, S. L. Craig, B. D. Olsen and J. A. Johnson, *Adv. Mater.*, 2024, **36**, 2406600.
12 S. Wang, S. Panyukov, M. Rubinstein and S. L. Craig, *Macromolecules*, 2019, **52**, 2772–2777.
13 S. C. Ligon-Auer, M. Schwentenwein, C. Gorsche, J. Stampfl and R. Liska, *Polym. Chem.*, 2015, **7**, 257–286.
14 R. O. Ritchie, *Nat. Mater.*, 2011, **10**, 817–822.
15 J. Dong, Z.-H. Zhao and C.-H. Li, *Chem. – Eur. J.*, 2025, **31**, e202404397.
16 A. P. Dhand, M. D. Davidson, H. M. Zlotnick, T. J. Kolibaba, J. P. Killgore and J. A. Burdick, *Science*, 2024, **385**, 566–572.
17 X. Yan, F. Wang, B. Zheng and F. Huang, *Chem. Soc. Rev.*, 2012, **41**, 6042–6065.
18 I. Onori, G. J. M. Formon, C. Weder and J. Augusto Berrocal, *Chem. – Eur. J.*, 2024, **30**, e202402511.
19 G. Men, W. Niu and X. Liu, *Chem. – Eur. J.*, 2025, **31**, e202500674.
20 J.-Y. Sun, X. Zhao, W. R. K. Illeperuma, O. Chaudhuri, K. H. Oh, D. J. Mooney, J. J. Vlassak and Z. Suo, *Nature*, 2012, **489**, 133–136.
21 S. Wang, Y. Hu, T. B. Kouznetsova, L. Sapir, D. Chen, A. Herzog-Arbeitman, J. A. Johnson, M. Rubinstein and S. L. Craig, *Science*, 2023, **380**, 1248–1252.
22 B. H. Bowser, S. Wang, T. B. Kouznetsova, H. K. Beech, B. D. Olsen, M. Rubinstein and S. L. Craig, *J. Am. Chem. Soc.*, 2021, **143**, 5269–5276.
23 H. Zhang, X. Li, Y. Lin, F. Gao, Z. Tang, P. Su, W. Zhang, Y. Xu, W. Weng and R. Boulatov, *Nat. Commun.*, 2017, **8**, 1147.
24 S. Dworakowska, F. Lorandi, A. Gorczyński and K. Matyjaszewski, *Adv. Sci.*, 2022, **9**, 2106076.
25 M. Chen, M. Zhong and J. A. Johnson, *Chem. Rev.*, 2016, **116**, 10167–10211.
26 S. C. Ligon, R. Liska, J. Stampfl, M. Gurr and R. Mülhaupt, *Chem. Rev.*, 2017, **117**, 10212–10290.
27 D. A. Rau, J. P. Reynolds, J. S. Bryant, M. J. Bortner and C. B. Williams, *Addit. Manuf.*, 2022, **60**, 103207.
28 ISO 37:2024(en), Rubber, vulcanized or thermoplastic---Determination of tensile stress–strain properties, **https://www.iso.org/obp/ui/#iso:std:iso:37:ed-7:v1:en**, accessed 19 August 2025.
29 E. Elmukashfi, *Sci. Rep.*, 2021, **11**, 16229.
30 C. Creton, *Macromolecules*, 2017, **50**, 8297–8316.
31 S. Perrier, *Macromolecules*, 2017, **50**, 7433–7447.
32 M. K. Boyajian, R. J. Lubner, L. O. Roussel, J. W. Crozier, B. A. Ryder and A. S. Woo, *Plast. reconstr. surg., Glob. open.*, 2019, **7**, 121.
33 M. Pensalfini, S. Meneghello, V. Lintas, K. Bircher, A. E. Ehret and E. Mazza, *J. Mech. Behav. Biomed. Mater.*, 2018, **77**, 711–717.
34 J. Yin, M. Li, G. Dai, H. Zhou, L. Ma and Y. Zheng, *J. Bionic Eng.*, 2021, **18**, 346–360.
35 M. Higgins, S. Leung and N. Radacsi, *Ann. 3D Print. Med.*, 2022, **6**, 100057.
36 O. Bliah, C. Hegde, J. M. R. Tan and S. Magdassi, *Chem. Rev.*, 2025, **125**(16), 7275–7320.
37 A. Zulifqar and M. Zeeshan, in *Handbook of Stretchable and Elastomeric Textiles*, ed. A. Zulifqar, Z. Khaliq and M. B. Qadir, Woodhead Publishing, 2024, pp. 163–210.
38 S. J. Melvin, Y. Yao, X. Huang, R. C. Bell, R. E. Kemmerling, I. Kevlishvili, A. C. Berg, A. P. Kitos Vasconcelos, A. Nelson, H. J. Kulik, S. L. Craig and R. S. Klausen, *J. Am. Chem. Soc.*, 2025, **147**, 6006–6015.